EAI Endorsed Transactions
on Energy Web

Research Article EAI.EU

Life Cycle Cost Modeling and Financial Benefit Assessment of Energy Storage Systems Incorporating Digital Twins

Lichang Zhang[1]*

[1] Jiaozuo Power Supply Company, State Grid Henan Electric Power Company, Jiaozuo 454000, China

Abstract

INTRODUCTION: Energy storage systems are increasingly evaluated under dynamic operating conditions in which battery degradation, efficiency decay, maintenance events, replacement timing, outage losses, and residual value jointly affect investment returns. However, conventional life-cycle cost and financial assessment methods mainly depend on static annual assumptions, making it difficult to explain how operational states are transformed into cost events and how these events change cash flow.

OBJECTIVES: This paper proposes a digital twin-driven economic health assessment model for life-cycle cost modeling and financial benefit evaluation of energy storage systems. Its main contribution is an economic state space that synchronizes SOC, SOH, temperature, depth of discharge, cycle count, conversion efficiency, alarm records, maintenance status, and life-cycle stage labels with cost-event generation.

METHODS: A window-level state mapping mechanism is further developed to identify available capacity, degradation level, efficiency loss, maintenance and replacement triggers, outage costs, and residual value recovery, and to aggregate them into annual cost streams. Based on the same cost streams and scenario revenue parameters, NPV, IRR, PBP, and LCOS are calculated through a unified financial evaluation chain.

RESULTS: Experiments on an industrial energy storage project show that the proposed model achieves an SOH mean absolute error of 0.82%, a total life-cycle cost error of 2.18%, an NPV of 7.18 million yuan, and an LCOS of 0.533 $RMB \cdot kWh^{-1}$ under the cost-aware dynamic operating strategy.

CONCLUSION: The results demonstrate that the model improves the traceability and adaptability of energy storage economic assessment and provides analytical decision support for dispatch and maintenance planning; automatic actuation of the physical asset is outside the scope of the present study.

Keywords: digital twin; energy storage system; life-cycle cost; financial benefit assessment; cost flow generation algorithm

Received on 06 July 2026, accepted on 24 August 2026, published on 17 September 2026

doi: 10.4108/ew.13900

1. Introduction

Digital twins, time-series prediction, and multisource data fusion are changing the economic evaluation of energy storage systems. Energy storage plants continuously generate data from BMS, PCS, EMS, metering and billing, and O&M activities during operation. These data not only reflect SOC, SOH, temperature, power and efficiency, but also have a direct impact on capacity degradation, lifetime loss, maintenance and replacement costs, downtime and residual value after decommissioning. In scenarios including

*Corresponding author. Email: ZLC202607@163.com

RES integration, peak and valley filling, as well as ancillary services, there is a strong correlation between the revenue generation capacity of the energy storage system and the degradation process; therefore, the development of a dynamic cost modeling approach based on operational data is required.

Current research focuses on three fields: Digital Twin Modeling, Battery Health Estimation, and Technology and Economic Evaluation of Energy Storage. Digital twin research focuses on establishing data mappings between physical battery systems and virtual models. Naseri et al. summarized a digital twin framework for battery systems from the perspectives of use cases, platform requirements, and data exchange [1]. Semeraro et al. analyzed the application pathways of digital twin in condition monitoring, O&M decision making, and trend prediction for energy storage systems [2]. Salaorni et al introduced digital twins into microgrid battery power storage systems, demonstrating their applicability in system management [3]. Regarding the state of health (SOH) estimation, Safavi et al. considered SOH estimation to be the key basis for building battery digital twins [4], whereas Wongdet et al. considered the lifetime factors of battery life in microgrid capacity configuration, showing that the degradation process has a direct impact on the energy storage capacity and cost results [5]. Regarding the economic assessment, Stanchev and Hinov compared the differences between LLL-based, Lead-Acid, and Hydrogen Energy Storage [6]; Migliari et al. calculated the Levelized Cost of Storage (LCOS) of BESS in the context of mitigation of PV reduction [7]; and Mulder and Klein compared different energy storage solutions in all-renewable energy systems [8]. However, the existing approaches remain separated at the methodological level. Data-driven degradation models predict SOH or remaining life but generally stop at the health-state output, while conventional dynamic life-cycle cost methods introduce degradation through annual coefficients or scenario assumptions without retaining the operating window, event source, and lifecycle stage. Digital twin studies support condition monitoring and O&M analysis, yet the intermediate mechanism that converts synchronized operating states into traceable economic events is still insufficiently defined. Consequently, existing methods do not provide a unified chain that maps multidimensional operating states to economic states, organizes discrete maintenance, replacement, outage, and retirement events, and then updates cost-sensitive decision information over successive evaluation cycles. To clarify the methodological distinction between the proposed model and related studies, Table 1 compares their state representation, degradation–cost coupling, event organization, cost-flow granularity, and feedback functions.

Table 1. Comparison between Related Studies and the Proposed Method

Study	Main research focus	Economic state space	Cost-event organization	Cost-flow granularity	Feedback function
Naseri et al. [1]	Battery digital twin use cases, requirements, and platforms	Operational and health-state representation	Not explicitly defined	Not focused on economic cost flow	Digital twin application framework
Semeraro et al. [2]	Condition monitoring, O&M decision making, and trend prediction	Equipment-state monitoring	Not explicitly defined	Not focused on lifecycle financial aggregation	O&M decision support
Salaorni et al. [3]	Digital twin management of battery storage in microgrids	Physical–virtual battery-state mapping	Not explicitly defined	System-management level	Microgrid management support
Wongdet et al. [5]	Battery lifetime, capacity configuration, and cost analysis	Lifetime-related parameters	Replacement treated through planning assumptions	Project or annual level	Capacity-planning output
Migliari et al. [7]	LCOS assessment for PV-curtailment mitigation	Scenario and economic parameters	Cost items aggregated in LCOS	Annual or project level	Financial comparison
Proposed method	Digital twin-driven economic health assessment	Joint representation of operation, degradation, alarms, maintenance, and lifecycle stages	Window-level cost-event queue with event ID and source tags	Window-level generation and annual aggregation	Model-side analytical feedback for dispatch and maintenance recommendations

In view of these shortcomings, this study develops a digital twin-driven economic health assessment model for life-cycle cost modeling and financial benefit evaluation of energy storage systems. The model transforms equipment-side operating data into dynamic financial inputs and addresses unclear cost-event triggers, insufficient degradation-cost accounting, and static financial assumptions. Its feedback function is limited to updating model-side economic states and generating traceable recommendations for dispatch, maintenance, and investment decisions, rather than automatically controlling the physical energy storage system.

2. A Full Life-Cycle Economic Evaluation Framework for Energy Storage Systems Incorporating Digital Twins

2.1. Defining the Scope of Full Life-Cycle Economic Evaluation for Energy Storage Systems

Economic assessment of energy storage systems includes the assets of the installation, the operating state, the decomposition process and the disposal of the end of the life. Describing a project cost in terms only of initial investment or average annual O&M costs obscures the cumulative effect of decreasing capacity, decreasing efficiency, and replacing downtime. Fixed investments are made during the construction and commissioning phase for battery packs, PCS, BMS, EMS, fire-fighting and temperature control systems, civil engineering and installation, and network connectivity; during the operational and operational phases, the cost of charging and discharging losses, the power consumption of ancillary equipment, inspection and maintenance, as well as the management of dispatch; the deterioration and maintenance stage is influenced by the deterioration of health status (SOH), increased depth of discharge (DOD), temperature variations, and increasing cycle number, which leads to a decrease in available capacity and an increase in life span; the replacement and life extension phase involves the replacement of a battery, a derailing operation, and a shutdown for maintenance; the decommissioning and recycling stage comprises the disposal and disposal of the remaining value, as well as the value of the secondary use [9]. To allow the integration of the economic objects of the various stages into a single assessment framework, this paper presents the economic objectives of the Energy Storage System as a phased set:

$$O_L = \{S_0 : C_0, S_1 : C_{op}, S_2 : C_{deg}, S_3 : (C_{rep}, C_{down}), S_4 : (C_{eol}, C_{rv})\} \quad (1)$$

where O_L denotes the set of economic objects for the entire life cycle of the energy storage system; S_0 through S_4 represent the construction and commissioning, operation and service, degradation and maintenance, replacement and life extension, and decommissioning and recycling phases, respectively; C_0 denotes the initial investment; C_{op} denotes the operating and service costs; C_{deg} denotes degradation-related costs; C_{rep} denotes replacement costs; C_{down} denotes downtime losses; C_{eol} denotes decommissioning and disposal costs; and S_{rv} denotes residual value recovery. This set of objects defines the scope of the economic evaluation of energy storage systems as a combination of phases, states, and cost events [10].

2.2. Overall Architecture of Digital Twin-Driven Economic Evaluation

As soon as the economic objectives are defined, the assessment framework needs to translate the traffic data produced by the PEMS into state inputs that can be identified through an economic assessment [11]. It consists of a physical energy storage layer, data acquisition layer, digital twin state layer, economic mapping layer, financial evaluation layer, and analytical decision-support feedback layer, finance layer, and feedback scheduling layer. The physical energy storage layer consists of a battery cluster, PCS, BMS, EMS, temperature control and fire suppression system, and grid connection metering means, and provides data on voltage, current, power, temperature, SOC, SOH, charge/discharge energy, efficiency, cycle count, and alarm records. Data acquisition layer performs time alignment, anomaly filtering, loss imputation, and window aggregation on multiple sources of data, so that the scale difference between BMS second level sampling, EMS scheduling cycle, and financial assessment cycle is eliminated. The Digital Twin State Layer synchronizes the operating and degraded states of the energy storage system, identifying whether the system is in normal operation, deterioration warning, substitution activation, or decommissioning and recycling phases [12]. The Financial Evaluation Layer uses a uniform time window to compute the cost flow, the revenue parameters, and the evaluation metrics. Figure 1 illustrates the digital twin-driven economic health assessment framework. Operational state recognition provides the input, economic state mapping and cost-flow generation form the intermediate process, and financial assessment and decision recommendations constitute the output. The feedback layer writes assessment results and recommended operating constraints back to the model-side state database for subsequent evaluation cycles. These recommendations require operator review and are not automatically issued to the PCS, BMS, or EMS in the current implementation.

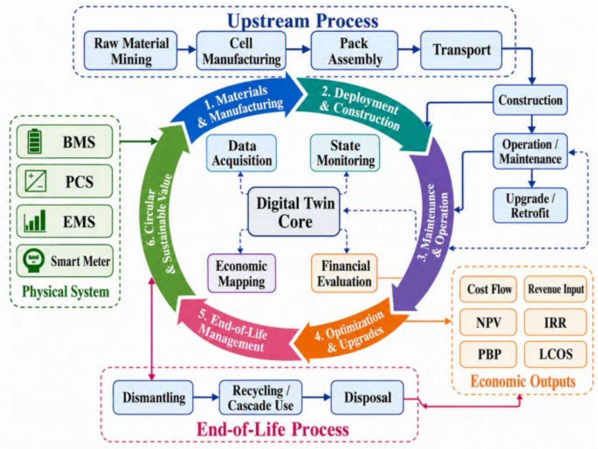

Figure 1. Framework for the Full Life Cycle Economic Evaluation of Energy Storage Systems Driven by Digital Twins

2.3. State Space of the Energy Storage System Digital Twin

As soon as the overall structure of the data flow is clarified, the state space further defines the variable forms by which the operating state enters the economic assessment. The Digital Twin State of the Energy Storage System shall at the same time represent the electrical performance, performance deterioration, cost triggers and life-cycle phases, and ensure that operating parameters, like SOC and SOH, are not limited to facility monitoring. Electric operation variables describe the process of energy exchange, such as SOC, power, voltage, current, charge, and discharge. Performance deterioration variables describe the process of consumption of the asset, including SOH, DOD, equivalent cycle count, temperature offset, and transformation efficiency; cost trigger variables describe the circumstances in which economic events take place, including alarm state, maintenance state, and phase label [13]. To ensure consistency between operational status and economic evaluation criteria, this paper represents the digital twin state within the evaluation window at t as:

$$x_t = \left[SOC_t, SOH_t, T_t, P_t, I_t, V_t, DOD_t, N_t, \eta_t, E_{ch,t}, E_{dis,t}, A_t, M_t, s_t\right] \quad (2)$$

where x_t represents the digital twin state vector of the energy storage system within the t th evaluation window; SOC_t represents the state of charge; SOH_t represents the state of health; T_t represents the temperature; P_t represents the charge and discharge power; I_t and V_t represent the current and voltage, respectively; DOD_t represents the depth of discharge; N_t represents the equivalent cycle count; η_t represents the conversion efficiency; $E_{ch,t}$ and $E_{dis,t}$ represent the charge and discharge quantities, respectively; A_t represents the alarm status; M_t represents the maintenance status; and s_t s_t represents the lifecycle stage label [14]. This state space integrates equipment operation parameters, degradation parameters, and phase tags into a single assessment framework, which allows the identification of capacity degradation, lifetime loss, maintenance warning, substitution triggers, decommissioning and recycling as economic assessment variables.

3. Digital Twin-Driven Lifecycle Cost–Financial Benefit Coupled Modeling Method

3.1. Cost-Flow-Driven Evaluation Logic Based on Twin States

The digital twin state vector cannot be directly used in financial evaluation because its variables have different physical meanings and sampling scales [15]. For each evaluation window ttt, synchronized observations from the BMS, PCS, EMS, and metering system are normalized, masked for missing values, and truncated only for nonphysical outliers to form x_t . The state mapping is therefore defined as a hybrid predictor-rule operator $F_\theta(\cdot;\Omega)$, where θ denotes the parameters of the TCN-GRU predictor and degradation classifier, and $\Omega = \left\{\tau_{SOH}^{rep}, \tau_T, \tau_\eta\right\}$denotes the rule thresholds fixed before testing. Its output is

$$z_t = F_\theta(x_t;\Omega) = \left[\hat{E}_{ava,t}, \hat{D}_t, \hat{\eta}_t, \hat{B}_t, \hat{K}_t\right] \quad (3)$$

The continuous economic states are obtained by

$$\hat{E}_{ava,t} = E_N \overline{SOH}_t \hat{\eta}_t, \quad \hat{D}_t = \underset{d\in\{0,1,2,3\}}{\arg\max}\, p_\theta(d|x_{t-L+1:t}),$$

$$\hat{B}_t = \min(\hat{E}_{ava,t}, B_t^{sch})$$

(3a)

where d=0,1,2,3 denotes healthy operation, degradation warning, replacement critical, and retirement candidate, respectively. The alarm variable ata_{t}at is coded as 0 for normal, 1 for warning, 2 for fault, and 3 for trip, while mt=1m_{t}=1mt=1 indicates that a shutdown maintenance record is active. The event vector $\hat{K}_t = \left[k_t^{mai}, k_t^{rep}, k_t^{out}, k_t^{der}\right]$is determined by

$$k_t^{mai} = \mathrm{II}(a_t \ge 1 \vee |T_t - T_{ref}| \ge \tau_T)$$

$$k_t^{rep} = \mathrm{II}(\overline{SOH}_t \le \tau_{SOH}^{rep} \vee (\hat{D}_t \ge 2 \wedge a_t \ge 2)) \quad (3b)$$

$$k_t^{out} = \mathrm{II}(a_t = 3 \vee m_t = 1)$$

$$k_t^{der} = \mathrm{II}(\hat{\eta}_t \le \tau_\eta \vee \hat{B}_t < B_t^{sch})$$

Accordingly, warning and temperature-deviation records enter the maintenance queue, fault records combined with critical degradation enter the replacement queue, trip or shutdown records generate outage costs, and efficiency or available-capacity violations activate derated-operation costs. Efficiency decay is not assigned an empirical LCOS penalty; it first produces the incremental loss cost $\Delta C_{\eta,t} = p_t^{ch} E_t^{dis} (\frac{1}{\hat{\eta}_t} - \frac{1}{\eta_0})$, which is accumulated into LCOS as

$$\Delta LCOS_\eta = \frac{\sum_{y=0}^{Y} \sum_{t \in \tau_y} \Delta C_{\eta,t} (1+r)^{-y}}{\sum_{y=0}^{Y} E_y^{dis} (1+r)^{-y}} \quad (3c)$$

Here, E_N is the rated energy capacity, B_t^{sch} is the scheduled settlement capacity, T_{ref} is the reference operating temperature, η_0 is the commissioning efficiency, p_t^{ch} is the charging-side electricity price. When any component of $\hat{K}_t$ changes from 0 to 1, the event index $I_{t,s,k}$ is written to the Cost Event Queue; consecutive windows with the same equipment ID and event type are merged to prevent repeated cost recognition [16]. The thresholds in Ω are taken from the project BMS alarm table, battery replacement specification, and PCS acceptance records and remain unchanged during test-set evaluation.

3.2. Dynamic Generation Model for Full Life-Cycle Costs

3.2.1. Determination of Initial Investment Cost Boundaries

The first node in the Cost Event Queue comes from the Construction and Commissioning Stage. The assets that are created in this phase have a clear definition of the project boundaries, such as the battery cluster, the power transfer system, the battery management system, the energy management system, the fire-extinguishing and temperature-control system, the grid connection, the installation, commissioning, and acceptance of the project. The algorithm reads equipment ledgers, contract lists, grid connection documents, and commissioning records during the project initialization. To avoid mixing operational-phase costs with asset investments, the initial investment is recorded only at the "$y = 0$" time point and is not included in window-level rolling updates. At the same time, the power rating, the design cycle life, the initial efficiency, and the commissioning date are written into the digital twin to be used as a reference for the subsequent state update. The initial investment range shall be consolidated on the basis of the composition of the installation:

$$C_0 = C_{bat} + C_{pcs} + C_{bms} + C_{ems} + C_{aux} + C_{gird} + C_{ins} \quad (4)$$

Where C_0 represents the initial investment cost of the energy storage system; C_{bat} represents the battery cluster cost; C_{pcs} represents the power conversion system cost; C_{bms} represents the battery management system cost; C_{ems} represents the energy management system cost; C_{aux} represents the cost of fire protection, temperature control, and safety support systems; C_{gird} represents the grid connection cost; and C_{ins} represents the installation and commissioning cost [17].After initialization, the cost database contains structured records in the format "Asset Item—Equipment ID—Rated Parameters—Commissioning Date—Discounting Period." All cost events generated during the operational service phase are linked to the asset boundary via the equipment ID.

3.2.2. Identification of Operational Degradation States

After the energy storage system enters operation, cost generation changes from static asset registration to window-level degradation recognition. BMS, PCS, EMS, and O&M records are aligned to the 15-min evaluation interval. For each interval, the input vector contains ten features: SOC, historical SOH, mean pack voltage, current, mean temperature, DOD, equivalent cycle increment, signed charge-discharge power, conversion efficiency, and alarm severity. Continuous features are standardized using the mean and standard deviation of the training set, while the alarm state is encoded from 0 to 3 for normal, warning, fault, and trip conditions. The historical input is constructed as $X_t = [x_{t-L+1}, \ldots, x_t] \in R^{L \times 10}$, $L = 96$, where 96 consecutive intervals correspond to 24 h of operation. The TCN contains three residual causal-convolution blocks with 32, 64, and 64 output channels, respectively [18]. The kernel size is 3, the dilation factors are 1, 2, and 4, and a dropout rate of 0.20 is applied after each residual block. The extracted temporal features are passed to a two-layer GRU with 64 hidden units per layer and a dropout rate of 0.20. The final GRU state is mapped through a 32-unit fully connected layer to obtain the one-step-ahead SOH prediction:

$$\overline{SOH}_{t+1} = f_\theta(X_t) \quad (5)$$

The model is trained jointly for SOH regression and degradation-state classification. The classifier receives the predicted SOH together with DOD, temperature deviation, equivalent cycle count, conversion efficiency, and alarm severity, and outputs the probabilities of healthy operation, degradation warning, replacement critical, and retirement candidate through a Softmax layer:

$$\hat{D}_t = \arg\max_{d \in \{0,1,2,3\}} p_\theta(d \mid \overline{SOH}_t, DOD_t, \Delta T_t, N_t, \eta_t, a_t), \quad (6)$$

The training objective combines the Huber regression loss and class-weighted cross-entropy:

$$L = L_{Huber}(\overline{SOH}, SOH) + \lambda_c L_{WCE}(\hat{p}, y), \quad \lambda_c = 0.30 \quad (6a)$$

Adam is used with an initial learning rate of 1.0×10^{-3}, a weight decay of 1.0×10^{-5}, and a batch size of 64. Training is limited to 200 epochs. The learning rate is reduced by a factor of 0.5 when the validation SOH MAE does not improve for eight epochs, and training is terminated after 15 epochs without improvement [19]. The checkpoint with the lowest validation SOH MAE is retained. The resulting degradation label is then written into the Cost Event Queue for maintenance, replacement, outage, and end-of-life cost identification.

3.2.3. Conversion of Capacity Loss and Lifespan Depletion

Once the degradation level has been marked as complete, the algorithm must convert the equipment state into an economic measure that can be integrated into the cost stream. Capacity is calculated from the nominal capacity; by combining the forecast SOH and the efficiency state, the actual available capacity can be derived. The efficiency element is included in the capacity transfer, since, for the same nominal capacity, the decrease in the conversion efficiency decreases the effective output power and also changes the cost per unit of discharge. The actual available capacity shall be updated based on the state of the window:

$$\hat{E}_{ava,t} = E_{rated} \cdot \overline{SOH}_t \cdot \eta_t \quad (7)$$

where $\hat{E}_{ava,t}$ represents the predicted effective available capacity within the th evaluation window (t), and E_{rated} represents the rated capacity. This value is written to the revenue capacity constraint field $\hat{B}_t$, which is used to limit the effective scope for participating in peak off-peak arbitrage, capacity compensation, and ancillary service settlement.

The part of the decrease in capacity shall be recorded separately as a loss amount and shall be used for the calculation of the change in the distribution of costs and the reduction of the service capacity due to the loss of capacity:

$$\Delta E_{loss,t} = E_{rated} - \hat{E}_{ava,t} \quad (8)$$

where $\Delta E_{loss,t}$ represents the capacity loss within the t th evaluation window. If $\Delta E_{loss,t}$ continues to increase within the same evaluation cycle, the cost event queue will raise the priority of the degradation warning status and write the cumulative capacity loss value to the annual cost buffer.

Lifetime depletion accounting addresses asset degradation caused by cycling. In this algorithm, the effective discharge capacity, the discharge depth, the temperature, the cycle number, and the predicted SOH are obtained, and a non-linear degradation correction function is used to calculate the lifetime depletion cost:

$$C_{deg,t} = k_{deg} E_{dis,t} \phi(DOD_t, T_t, N_t, \overline{SOH}_t) \quad (9)$$

where $C_{deg,t}$ represents the lifespan depletion cost within the th evaluation window (t), k_{deg} represents the degradation cost coefficient per unit of net discharge capacity, $E_{dis,t}$ represents the net discharge capacity, and $\phi(DOD_t, T_t, N_t, \overline{SOH}_t)$ represents the degradation correction function determined jointly by depth of discharge (DOD), temperature, equivalent cycle count, and state of health (SOH) [20]. This calibration function is calibrated with historical maintenance records and capacity validation results, assigning a higher life loss weight to a high DOD, a high temperature, and a high cycle frequency.

The cost of energy loss due to a decrease in efficiency shall be calculated at the same time in the same time frame. In this algorithm, the cost of charging, charging, discharging, discharging, and efficiency are taken as input to calculate the equivalent loss cost in the charging and discharging process:

$$C_{loss,t} = p_{ch,t} E_{ch,t} - p_{dis,t} E_{dis,t} \eta_t \quad (10)$$

In the equation, $C_{loss,t}$ represents the energy loss cost within the th evaluation window (t), $p_{ch,t}$ represents the charging-side electricity price, $E_{ch,t}$ represents the amount of energy charged, $p_{dis,t}$ represents the discharging-side electricity price, and $E_{dis,t}$ represents the amount of energy discharged. Capacity loss, lifespan depletion, and energy loss are each assigned to different cost fields; source labels are retained during annual aggregation to facilitate itemized verification of degradation cost errors, loss cost errors, and total cost errors in the experimental section [21].

3.2.4. Triggers for Maintenance, Replacement, and Outage Costs

Following the conversion of continuous degradation costs, discrete event costs are jointly triggered by the degradation level, alarm state, and maintenance record. Maintenance, replacement, outage, and derated-operation costs are not assigned using fixed annual percentages; instead, event conditions are checked within each evaluation window. The event set is defined as $E = \left\{e^{mai}, e^{rep}, e^{out}, e^{der}\right\}$, representing maintenance, component replacement, outage, and derated operation, respectively. For each event type j, the trigger region R_j is determined from the manufacturer-specified SOH replacement limit, permissible temperature and efficiency ranges, and lifecycle-stage criteria, whereas the alarm threshold τ_j is taken from the BMS/PCS alarm tables and the project O&M manual. Historical operating data from the training and validation periods are used only to verify the consistency of these engineering boundaries and to resolve overlapping event conditions; the thresholds are not learned directly by the TCN-GRU model. When the degradation state enters R_j or the alarm severity reaches τ_j, the event flag is set to 1:

$$k_t^j = \mathrm{II}(\hat{D}_t \in R_j \vee a_t \geq \tau_j) \quad (11)$$

where k_t^j represents the trigger flag for event type j within evaluation window t. Warning-level alarms or violations of the permissible temperature and efficiency ranges trigger maintenance or derated-operation checks; a fault-level alarm combined with the replacement-critical degradation state triggers component replacement; and a trip alarm or an active shutdown record triggers outage-cost recognition. All trigger regions and alarm thresholds are fixed before test-set evaluation, and identical events occurring in consecutive windows are merged using the equipment ID and event type to prevent repeated cost recognition.

The algorithm reads the relevant cost field according to the event identifier as soon as a trigger event enters the cost synthesizer [22]. The cost of maintenance is based on O&M records and inspection schedules; the cost of replacement is based on the price of a battery pack or a PCS component; the cost of downtime is estimated from the downtime period and the service loss; and the operating cost is calculated from the reduction in available capacity and scheduling constraints. The cost summary for window events is as follows:

$$C_{even,t} = I_{mnt,t}C_{mnt,t} + I_{rep,t}C_{rep,t} + I_{down,t}C_{down,t} + I_{der,t}C_{der,t} \quad (12)$$

where $C_{even,t}$ represents the event cost within the th evaluation window (t), $I_{mnt,t}, I_{rep,t}, I_{down,t}, I_{der,t}$ denote the event identifiers for maintenance, replacement, downtime, and derated operation, respectively, and $C_{mnt,t}, C_{rep,t}, C_{down,t}, C_{der,t}$ denote the corresponding event costs. The Event Cost Record also stores the Device ID, Trigger Time, Degradation Level, Warning Type, and Cost Source to avoid repeating the same Error Count on Neighboring Windows. If the event spans more than one window, the system will consolidate the records according to the event ID and determine the financial year for which the cost is assigned.

3.2.5. Decommissioning and Residual Value Recovery Entry

When the lifecycle stage label changes to"S_4," the cost flow shifts from operational-phase events to net decommissioning costs. The decommissioning decision shall be based on the assessment period, the lower health status (SOH), capacity validation results and safety status [23]. When the battery pool fulfils the decommissioning criteria, the algorithm will cease generating the cost of normal operating windows and will switch to the decommissioning record table to obtain dismantling, transport, security checks, compliant disposal, recovery and second use assessments. At the end of the process, the costs of the decommissioning phase are generally recorded centrally and include compensation for the recovery of the residual value; thus, they are recorded as net costs in the cost stream:

$$C_{eol,T} = C_{dis,T} + C_{tr,T} + C_{safe,T} - S_{rv,T} \quad (13)$$

where $C_{eol,T}$ represents the net decommissioning cost at the end of the evaluation period, $C_{dis,T}$ represents the dismantling and disposal cost, $C_{tr,T}$ represents the decommissioning transportation cost, $C_{safe,T}$ represents the safety inspection and compliance processing cost, and $S_{rv,T}$ represents the revenue from residual value recovery or secondary utilization of materials. If the remaining capacity of the battery in the decommissioning assessment table meets the conditions for secondary utilization, $S_{rv,T}$ is recorded based on the secondary utilization value; if the safety inspection does not meet the conditions for reuse, $S_{rv,T}$ retains only the residual value field.Net decommissioning costs are tied to the asset ID to prevent replacement battery packs and original battery packs from being double-counted in residual value recovery.

3.2.6. Annual Cost Stream Integration

After window-level cost events are written, the cost aggregator reads operating costs, energy losses, lifespan consumption, event costs, and net decommissioning costs according to the annual index Ω_y .Different cost items keep their source tags in the database; both the total and the itemized cost flows are generated at the same time during the year aggregation [24]. The operational and power losses are aggregated window by window; the degradation costs are accumulated on the basis of the actual discharge and the corrective weights; the event costs are consolidated by the event identification and assigned to the relevant year; and the net decommissioning costs are recorded only at the end of the assessment period or in the year in which decommissioning takes place. Figure 2 shows the process of triggering the full life cycle cost event and generating the cost flow. The process starts with the reading of data from the twin state, proceeds to SOH prediction, degradation level determination, capacity loss transformation, event trigger check, shutdown entry, and yearly cost cache update, and finally generates an annual cost stream that can be used to evaluate financial benefits.

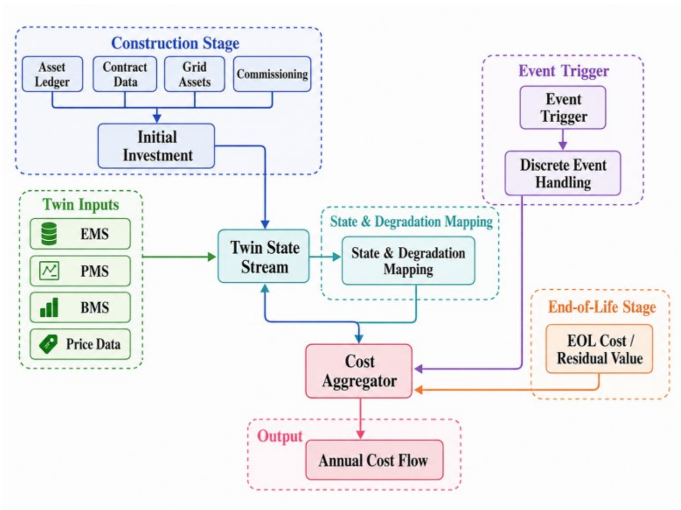

Figure 2. Flowchart of Full Life-Cycle Cost Event Triggering and Cost Stream Generation

3.3. Cost-Stream-Driven Financial Benefit Evaluation Algorithm

3.3.1. Integration of Cost Streams and Scenario Revenue Parameters

Once the annual cost flow is generated, the financial evaluation module reads the revenue parameters from the project electricity-settlement records, ancillary-service clearing statements, and EMS dispatch schedules. These parameters are fixed for all operating strategies rather than optimized separately by the proposed method. For the industrial-park case, the peak and valley electricity prices are set to 1.02 and 0.32 RMB·kWh⁻¹, respectively, corresponding to a peak-valley spread of 0.70 RMB·kWh⁻¹. The ancillary-service capacity and mileage clearing prices are 28 RMB·MW⁻¹·h⁻¹ and 5.6 RMB·MW⁻¹, respectively. The discount rate and evaluation horizon are fixed at 6% and 15 years. The same price series, settlement rules, and annual escalation assumptions are used for all four strategies.

Capacity degradation constrains revenue through the eligible energy and power rather than by directly changing the market price. For evaluation window ttt, the settlement boundaries are defined as

$$E_t^{elig} = \min(E_t^{sch}, E_N \overline{SOH}_t \hat{\eta}_t)(1-k_t^{out}),$$
$$P_t^{elig} = \min(P_t^{sch}, P_N \hat{\eta}_t)(1-\delta k_t^{der}), \quad \delta = 0.20 \tag{14}$$

where E_t^{sch} and P_t^{sch} are the scheduled settlement energy and power, E E_N and P_N are the rated energy and power, and k_t^{out} and k_t^{der} denote outage and derated-operation events.

Peak-valley arbitrage and ancillary-service revenues are then calculated as

Rtarb=ptpeakEtdis,elig−ptvalleyEtch,RtAS=πtcapPteligΔt+πtmilMtelig.R_{t}^{\mathrm{arb}} =

$$R_t^{arb} = p_t^{peak} E_t^{dis,elig} - p_t^{valley} + E_t^{ch},$$
$$R_t^{AS} = \pi_t^{cap} P_t^{elig} \Delta t + \pi_t^{mil} M_t^{elig} \tag{15}$$

Accordingly, a decline in SOH or efficiency reduces the eligible discharge energy and ancillary-service capacity, while outage and derating events suspend or proportionally reduce the corresponding revenue. The dynamic optimization strategy changes only the accepted operating windows and dispatch quantities; it does not use higher electricity prices or clearing prices than the comparison strategies.

3.3.2. Rolling Calculation of Net Cash Flow

After the cost stream and revenue parameters are aligned by year, the rolling cash flow module updates the financial evaluation cache on an annual basis. The cash flow for year y is derived by subtracting the lifecycle cost stream from the scenario's revenue parameters for that same year. Since the cost side is driven by window aggregation based on twin states, the cash flow curve changes dynamically in response to degradation status, event triggers, and decommissioning entries. When a replacement event is triggered in a given year, the event cost is recorded in C_y , causing a significant dip in the cash flow; if the SOH recovers to a higher range after replacement, the effective capacity and efficiency fields return to a healthy state in subsequent years, and the cash flow curve changes as capacity constraints are relaxed. During the rolling calculation process, the system retains the "NCF_y ," "Cumulative Net Cash Flow," "Discounted Net Cash Flow," and "Cost Source Breakdown" fields to facilitate identifying whether the decline in financial benefits stems from degradation costs, event costs, energy losses, or a contraction in revenue constraints [25]. If there are missing windows in the input data, the cash flow module reads the missing value mask and uses the states of adjacent windows and curves from similar operating days to interpolate the cost flow; it does not directly delete records for missing years.

3.3.3. NPV, LCOS, and Payback Period Outputs

Financial metric outputs utilize the same set of annual cost flows and revenue parameters to maintain consistency in inputs across NPV, IRR, PBP, and LCOS. During metric calculation, the initial investment C_0 is entered as an expenditure in Year 0; the annual cost flow C_y is provided by the cost generation algorithm; the annual revenue parameters R_y are imported from scenario settlement records; and the effective available discharge capacity $\hat{E}_{ava,y}$ is aggregated from window-level available capacity. Key metrics are output according to a unified calculation group:

$$
\begin{cases}
C_y = \sum_{t \in \Omega_y} (C_{op,t} + C_{loss,t} + C_{\deg,t} + C_{event,t}) + \Pi_{y=Y} C_{eol,T} \\
R_y = R_{arb,y} + R_{dem,y} + R_{cap,y} + R_{anc,y} + R_{ren,y} \\
NCF_y = R_y - C_y \\
NPV = -C_0 + \sum_{y=1}^{Y} \frac{NCF_y}{(1+r)^y} + \frac{S_{rv,Y}}{(1+r)^Y} \\
IRR: -C_0 + \sum_{y=1}^{Y} \frac{NCF_y}{(1+IRR)^y} + \frac{S_{rv,Y}}{(1+IRR)^Y} = 0 \\
PBP = \min \left\{ y : \sum_{\tau=1}^{y} NCF_\tau \geq C_0 \right\} \\
LCOS = \dfrac{C_0 + \sum_{y=1}^{Y} \frac{c_y}{(1+r)^y}}{\sum_{y=1}^{Y} \frac{\hat{E}_{ava,y}}{(1+r)^y}}
\end{cases} \tag{16}
$$

In the formula, C_y represents the life-cycle cost stream for year y ; Ω_y represents the set of evaluation windows included in year y ; $\Pi_{y=Y}$ represents the end-of-evaluation-period indicator; R_y represents the scenario revenue parameters for year y ; $R_{arb,y}, R_{dem,y}, R_{cap,y}, R_{anc,y}, R_{ren,y}$ represent the revenues from peak-valley arbitrage, demand response, capacity compensation, ancillary services, and renewable energy integration, respectively; NCF_y represents the annual net cash flow; r represents the discount rate; Y represents the evaluation period; $S_{rv,Y}$ represents the recovery of residual value at the end of the cycle; and $\hat{E}_{ava,y}$ represents the annual effective available discharge capacity.The indicator output table simultaneously records statistics on cost breakdown percentages, revenue scenario sources, capacity constraint statuses, and degradation levels; financial evaluation results can be traced back to specific cost events and operating windows .

3.4. Comprehensive Cost-Benefit Evaluation and Operational Feedback

Then, the algorithm advances to the integrated assessment and feedback stage. The NPV, IRR, PBP, LCOS, deterioration risk, event cost ratio, and capacity constraints are normalized to determine the project level cost-benefit status. Not only are the complex assessments stored in the form of financial statements, but they can also be broken down into operationally interpretable fields, such as high-loss windows, high-power loss windows, substitution risk windows, revenue reduction windows, and net cost-sensitive window closures. These fields are entered into a digital twin and are associated with device IDs, operating modes, DOD ranges, temperature ranges, and dispatch instructions. The feedback module reduces the priority of that segment in the dispatch plan if a specific operating segment corresponds to a high degradation cost; if the ancillary service revenue is high, but causes reduced operating costs, the feedback module adjusts the upper limit of response power and participation time slots; if the increase in the LCOS is mainly caused by a decrease in efficiency, the feedback module integrates the temperature control strategy, the PCS efficiency check, and the maintenance task into the O&M plan; if the net decommissioning costs have a significant impact on the financial results, the feedback module updates the residual value restoration parameters and records for the second utilization assessment.

Figure 3 shows the evaluation of financial benefits and operational feedback mechanisms based on cost flows. The left side reads the annual cost flow and scenario income parameters; the middle outputs NPV, IRR, PBP, and LCOS; the right-hand side generates scheduling, maintenance, and shutdown feedback based on the high cost and high risk segments, and the feedback results are rewritten into the digital twin state space. During the next cycle of operational data synchronization, the assessment results are fed into the status mapping module, together with the new SOC, SOH, temperature, efficiency, and alarm status, forming a closed loop computation chain of "status update — cost event — financial assessment — operational feedback."

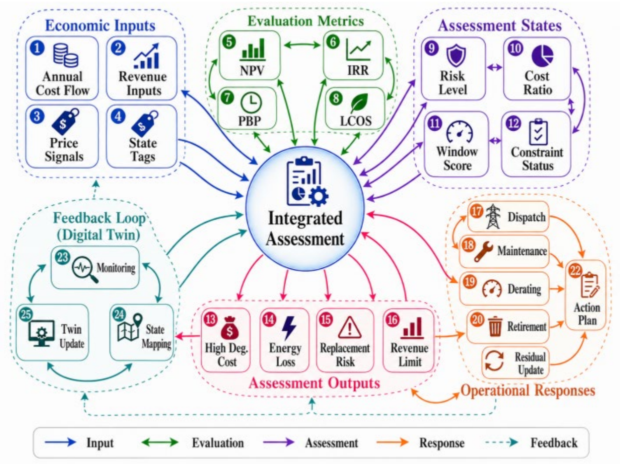

Figure 3. Diagram of the Cost-Flow-Driven Financial Benefit Assessment and Operational Feedback Mechanism

The operating strategy is implemented as a deterministic cost-aware screening procedure rather than as a mathematical optimization solver. For each 15-min evaluation window, the net operating value is calculated as

$$S_t = R_t^{elig} - C_t^{ene} - C_t^{\deg} - C_t^{evt} \quad (17)$$

where R_t^{elig} denotes the eligible peak-valley and ancillary-service revenue, C_t^{ene} is the energy-loss cost, $C_t^{\deg}$ is the lifespan-depletion cost, and C_t^{evt} is the expected maintenance, replacement, outage, or derating cost. Within each rolling 24-h horizon containing 96 evaluation windows, candidate windows are ranked according to S_t. A window is retained only when $S_t > 0$, the SOC remains within the EMS operating limits, the SOH is above the replacement threshold, and no outage event is active. When a derating event is detected, the eligible power is reduced according to Eq. (3.3.1). The procedure uses deterministic ranking and threshold filtering without an iterative optimization solver; therefore, it is defined as a cost-aware dynamic operating strategy.

4. Experimental Design and Results Analysis

4.1. Experimental Environment and Dataset Configuration

The experimental dataset was constructed from the operating records of a 2 MW/4 MWh lithium iron phosphate battery energy storage system in an industrial park. The measured data covered the period from January 1, 2023 to December 31, 2024, corresponding to 731 operating days and 70,176 original 15-min windows. After time alignment, missing-value processing, and data-quality screening, 68,160 valid evaluation windows and 568 equivalent full cycles were retained. The operation and maintenance records contained 21 maintenance events, three component-replacement events, including two battery-module replacements and one PCS component replacement, and 12 outage events. The data sources included the battery management system (BMS), power conversion system (PCS), energy management system (EMS), metering platform, and operation and maintenance records. BMS variables comprised SOC, historical SOH, pack voltage, current, temperature, and alarm status at a sampling interval of 1 s; PCS data included charge-discharge power, conversion efficiency, operating mode, and fault status at 5 s; EMS dispatch commands and settlement records were aggregated into 15-min evaluation windows. Missing ratios below 3% were interpolated using adjacent records from comparable operating days, whereas actual temperature excursions, fault alarms, outages, and communication interruptions were retained as event features.

The valid samples were divided chronologically into training, validation, and test sets at a ratio of 7:2:1, corresponding to 47,712, 13,632, and 6,816 evaluation windows, respectively, to prevent information leakage between adjacent windows. Each TCN-GRU input sequence contained 96 consecutive 15-min windows, corresponding to 24 h, with ten features: SOC, SOH, voltage, current, temperature, DOD, equivalent cycle increment, charge-discharge power, conversion efficiency, and alarm severity. The trigger regions and alarm thresholds in Eq. (11) were fixed before testing according to the battery manufacturer's replacement criteria, BMS/PCS alarm configuration tables, permissible temperature and efficiency ranges, and the project O&M manual. Training and validation data were used only to verify boundary consistency, while the test set was not used for threshold adjustment.

The projection was initialized using the final measured operating state, and representative monthly operating profiles extracted from the two-year dataset were applied in a rolling window simulation. Future SOH, available capacity, efficiency, and event states were updated iteratively by the trained TCN-GRU model and the event-trigger rules. Long-term cycle-life and replacement boundaries were taken from manufacturer specifications, maintenance and replacement costs were obtained from project contracts and O&M records, and electricity prices and ancillary-service revenues were derived from settlement statements. The principal model, threshold, and financial settings are summarized in Table 2.

Table 2. Main Configuration of the TCN-GRU Model and Event-Trigger Rules

Category	Parameter	Setting
Input	Evaluation interval	15 min
Input	Historical window	96 intervals (24 h)
Input	Number of features	10
TCN	Residual blocks	3
TCN	Output channels	32, 64, 64
TCN	Kernel size and dilation	3; 1, 2, 4
GRU	Layers and hidden units	2 layers; 64 units per layer
Regularization	Dropout	0.20
Training	Optimizer and learning rate	Adam; ($1.0*10^{-3}$)
Training	Batch size and maximum epochs	64; 200
Training	Loss function	Huber loss + weighted cross-entropy
Training	Early stopping	15 epochs
Trigger rules	Threshold sources	Manufacturer specifications, BMS/PCS alarm tables, and O&M manual
Operating strategy	Screening horizon	96 intervals (24 h)
Operating strategy	Solution procedure	Deterministic ranking and threshold filtering

The model was implemented in Python 3.10 with PostgreSQL for cost-event storage. Training was conducted on a workstation equipped with an Intel Xeon processor, 64

GB RAM, and an NVIDIA RTX 4090 GPU. Adam optimization, learning-rate reduction, and early stopping were applied according to Table 1, and the checkpoint with the lowest validation SOH mean absolute error was retained. State prediction was evaluated using MAE, RMSE, MAPE, and R^2, while cost-flow performance was assessed using total cost error, degradation cost error, replacement cost error, residual value error, and LCOS error. Financial performance was further measured using NPV, IRR, PBP, and LCOS.

4.2. Validation of Digital Twin State Prediction Performance

The precision of life cycle cost flow is determined by the precision of SOH, available capacity and transformation efficiency. In order to validate the capability of the state mapping module to identify the degradation and the cost event trigger, Table 3 shows the forecast results of the various models on the test set.

Table 3. Comparison of Digital Twin State Prediction Performance

Model	SOH MAE/%	SOH RMSE/%	Available Capacity MAPE/%	Efficiency MAE/%	Degradation Level Classification Accuracy/%	R^2
Static Degradation Model	2.84	3.61	4.92	2.31	78.4	0.842
LSTM model	1.46	1.89	2.73	1.28	86.7	0.925
GRU model	1.32	1.71	2.51	1.15	88.1	0.937
TCN model	1.18	1.55	2.24	1.08	89.5	0.946
Digital Twin State Prediction Model	0.82	1.07	1.63	0.76	93.2	0.971

Table 3 indicates that the static degradation model has a higher error in SOH and available capacity estimates, since it uses a fixed degradation rate that does not account for DOD, temperature and cycle count. LSTM, GRU and TCN can capture some of the time series degradation characteristics, reducing SOH MAE to 1.46%, 1.32%, and 1.18%, respectively; however, they do not make adequate use of the alarm state and the life cycle stage label, which leads to a degradation level accuracy rate of less than 90%. The digital twin state prediction model uses the operating state, the efficiency state, the alarm field, and the stage tag as a common input, reducing the SOH MAE to 0.82%, achieving a MAPE of 1.63% for usable capacity, and achieving a precision of 93.2% for degradation level identification. The results show that the candidate states needed to trigger cost events — health, alert, critical, and retirement — can be distinguished with a reasonable degree of stability, providing usable state inputs for subsequent cost flows.

4.3. Analysis of Life Cycle Cost Estimation Results

Cost estimation errors are mainly reflected in degradation cost, replacement cost, residual value, and LCOS after the predicted operating states are converted into economic inputs. To isolate the contribution of the economic aggregation strategy from that of the degradation prediction model, all comparison methods use the same SOH, available-capacity, efficiency, and degradation-level outputs generated by the proposed TCN-GRU model. The cost boundaries, discount rate, equipment prices, residual-value parameters, and test periods are also kept unchanged, while only the cost aggregation mechanism is varied. Table 4 compares the resulting life-cycle cost estimation errors under five economic aggregation strategies.

Table 4. Comparison of Life-Cycle Cost Estimation Errors under Different Economic Aggregation Strategies

Economic Aggregation Strategy	Common State Predictor	Total Cost MAPE/%	Degradation Cost Error/%	Replacement Cost Error/%	LCOS Error/%	Residual Value Error/%
TCN-GRU + Static Annualized LCC	TCN-GRU	6.83	8.96	15.24	7.42	10.86
TCN-GRU + Empirical Annual Degradation Allocation	TCN-GRU	5.41	6.87	11.35	5.96	9.12
TCN-GRU + SOH-Adjusted Annual Cost	TCN-GRU	4.36	4.98	8.47	4.62	7.21
TCN-GRU + Annual Event-Triggered Aggreg	TCN-GRU	3.31	4.26	5.14	3.72	5.63

ation						
TCN-GRU + Dynamic Window-Level Cost Flow (Proposed)	TCN-GRU	2.18	3.14	3.52	2.37	4.06

The static annualized LCC strategy distributes O&M and replacement costs using fixed annual coefficients; the empirical strategy adjusts annual degradation costs according to DOD and equivalent cycles; the SOH-adjusted strategy corrects annual capacity and degradation costs using the common TCN-GRU SOH output; and the annual event-triggered strategy identifies threshold events but aggregates them directly by year without the window-level event queue, event merging, or source-tagged cost flow used by the proposed method.

Table 4 shows that, under the same TCN-GRU state predictions, the static annualized LCC strategy produces a replacement-cost error of 15.24% because fixed yearly coefficients cannot represent concentrated replacement and outage events. Introducing empirical degradation allocation reduces the total cost MAPE to 5.41%, while SOH-adjusted annual aggregation further lowers it to 4.36%; however, both approaches retain annual averaging and therefore provide limited temporal localization of discrete costs. The annual event-triggered strategy reduces the replacement-cost error to 5.14%, confirming the value of threshold-based event identification, but its direct annual aggregation cannot fully preserve event duration, lifecycle stage, or cost-source information. The proposed dynamic window-level cost flow achieves a total cost MAPE of 2.18%, a replacement-cost error of 3.52%, and a residual-value error of 4.06%. Since all methods share the same degradation predictions, the remaining improvement can be attributed primarily to window-level event generation, event merging, and lifecycle-stage-aware cost aggregation. Figure 4 further presents the variation in the life-cycle cost composition across operating years.

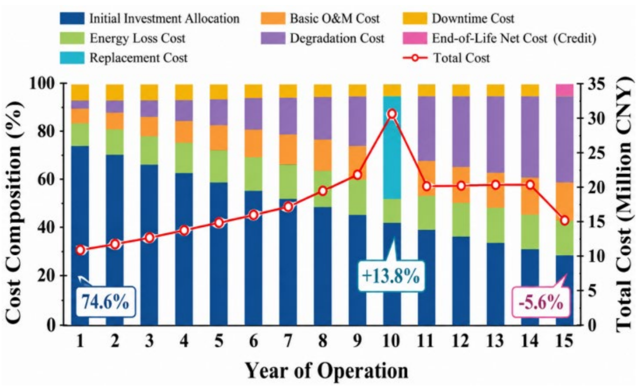

Figure 4. Changes in the Composition of Life-Cycle Costs over Different Operating Years

As shown in Figure 4, the percentage of initial investment in the initial stage of operation is the highest at 74.6 per cent in the first year. After five years of operation, the proportion of energy loss and base O&M costs has increased gradually to a total of 22.8 percent. After the eighth year, the cost of degradation increases more substantially, corresponding to a decrease in SOH and an increase in depth; the cost of replacement reaches its peak in the tenth year, when the total cost of the year is up 13.8% from the previous year; in the fifteenth year, the residual value of the decommissioning is compensated by 5,6% of the ELV costs. These changes in the cost structure show that the entire life cycle assessment has to take into account both the ongoing degradation and the discrete replacement events; the average cost per year does not reflect the variations in the cost of the subsequent phases.

4.4. Analysis of Financial Benefit Evaluation Results

Once the cost-flow calculations are completed, the return on investment, payback period, and unit discharge cost are compared. The four strategies include peak-valley arbitrage priority, ancillary-service priority, health-state constraint, and the cost-aware dynamic operating strategy. The latter applies the rolling net-value screening rule defined in Section 3.4 rather than solving a mathematical programming problem. The projected financial results are presented in Table 5.

Table 5. Financial Evaluation Results under Identical Revenue Assumptions

Operating Strategy	NPV (10,000 yuan)	IRR/ %	PBP/ year	LCOS/yuan·kWh $^{-1}$	SOH at End of Cycle/ %
Peak-Valley Arbitrage Priority	582.0	9.86	8.4	0.612	72.6
Priority for auxiliary services	644.0	10.31	8.1	0.596	70.8
Health Status Constraints	537.0	9.42	8.7	0.548	78.9
Cost-Aware Dynamic Operating Strategy	718.0	11.24	7.3	0.533	76.4

Table 5 shows that the ancillary-service-priority strategy achieves an NPV of 6.44 million yuan, but its end-of-cycle SOH decreases to 70.8% because frequent responses increase degradation and reduce subsequent eligible capacity. The health-constrained strategy maintains an end-of-cycle SOH of 78.9% and lowers LCOS to 0.548 RMB·kWh^{-1}, although fewer eligible settlement windows limit its NPV to 5.37 million yuan. The cost-aware operating strategy strategy jointly screens marginal revenue, degradation cost, and available-capacity constraints, resulting in an NPV of 7.18 million yuan, an IRR of 11.24%, a PBP of 7.3 years, and an LCOS of 0.533 RMB·kWh^{-1}. Because the four strategies use identical electricity prices, ancillary-service clearing prices, discount rates, and capacity-degradation equations, the observed financial improvement reflects differences in dispatch and cost-aware window selection rather than more optimistic revenue assumptions.

To further compare the balance among NPV, IRR, PBP, LCOS, and SOH retention under the common revenue assumptions, the normalized results are presented in Figure 5.

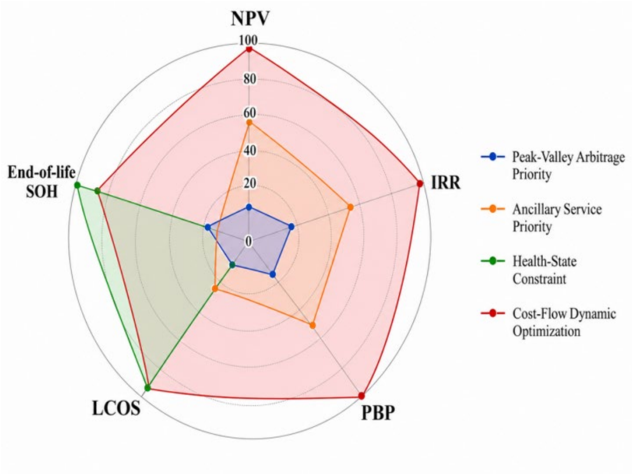

Figure 5. Multi-indicator radar chart of financial benefits under different operating strategies

As shown in Figure 5, the performance of the ancillary service priority strategy on the revenue side is strong, but the performance on the SOH and the risk control dimensions is lower; the Health Condition Constraint Strategy is superior in LCOS and SOH, but the revenue side is significantly lower; the Dynamic Cost Optimization Strategy keeps high consistency between NPV, IRR, PBP, LCOS, and SOH retention rate. Compared to Table 3, it is clear that the outcome of the evaluation of financial benefits is not determined by a single strategy with the highest return; the cost of degradation, substitution, and LTP may change the final ranking.

4.5. Ablation Experiment Analysis

The sensitivity and robust results show that the model is stable to some extent, but the contribution of each module to the assessment results needs to be verified separately. The SOH prediction module, lifecycle-stage label, cost-event trigger mechanism, and analytical decision-support feedback module were removed separately and compared with the complete model. The resulting changes in assessment performance are presented in Figure 6.

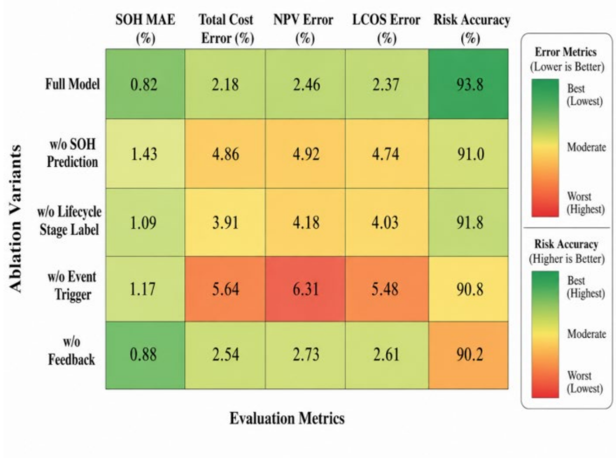

Figure 6. Changes in Evaluation Performance after Ablation of Different Modules

As shown in Figure 6, the full model has a SOH MAE of 0.82%, an overall cost error of 2.18%, a NPV error of 2.46%, an LCOS error of 2.37%, and a risk identification precision of 93.8% Taking away the SOH forecast module, the SOH MAE increased to 1.43%, and the total cost error increased to 4.86%, which showed that the degradation forecast had a direct impact on the estimation of the capacity loss and the life consumption. The total cost error was 5.64% and the NPV error went up to 6.31%. The main reason was that the cost of maintenance, replacement, and downtime was averaged, which did not account for the jump in cost due to the state threshold. After removal of the analytical feedback module, the state-prediction error remained almost unchanged, whereas risk-identification accuracy decreased to 90.2%. This reduction resulted from the absence of model-side historical cost-risk labels and updated economic constraints in subsequent assessment cycles. The result verifies the contribution of analytical state updating and decision support, but does not constitute evidence of automatic closed-loop control of the physical energy storage system. The results are in agreement with previous experiments: Digital twin state prediction, life cycle stage label, and cost event trigger collectively determine the computation precision of life cycle cost flow.

5. Conclusion

Full Life Cycle Economic Assessment of Energy Storage Systems with Digital Twins integrates the operational state, performance deterioration process and financial performance into one computing chain, moving the economic evaluation of energy storage projects from static to state-driven dynamic evaluation. The results show that digital twin variables — for example, SOC, SOH, temperature, cycle count, transformation efficiency, and alarm state — can be used to characterize the cost formation process effectively. Both the accuracy of the calculation of the life cycle and the stability of the financial assessment results are improved when the cost events — such as operating deterioration, loss of capacity, maintenance and replacement, shutdown and recycling, are continuously identified within a single time window, and the reliability of the financial assessment results are improved. The cost-driven approach more accurately reflects the interdependence between revenue generation, longevity depletion, and unit energy storage costs, so as to avoid the problems of early replacement costs, increasing LCOS, and longer payback periods that result solely from the pursuit of short term profit. The digital twin feedback system provides a more permanent foundation for the adjustment of the operating strategy, the establishment of the maintenance plan, and the assessment of the value of the decommissioning. This study still has limitations due to its emphasis on one energy storage scenario and limited operating cycle data; its applicability to various types of batteries, market mechanisms, and coordinated operating conditions at multiple sites needs to be validated. Future work could include the establishment of cross-scenario twin models for multiple energy storage systems, including real time electricity prices, carbon trading revenues, and equipment health management data, to further develop a cloud-edge collaborative economic assessment platform for energy storage assets throughout their lifecycle.

References

[1] Naseri F, Gil S, Barbu C, et al. Digital twin of electric vehicle battery systems: Comprehensive review of the use cases, requirements, and platforms[J]. Renewable and Sustainable Energy Reviews, 2023, 179: 113280.

[2] Semeraro C, Olabi A G, Aljaghoub H, et al. Digital twin application in energy storage: Trends and challenges[J]. Journal of Energy Storage, 2023, 58: 106347.

[3] Salaorni D, Bianchi F, Colnago S, et al. A novel digital twin for battery energy storage systems in microgrids[J]. Journal of Energy Storage, 2025, 132: 117745.

[4] Safavi V, Bazmohammadi N, Vasquez J C, et al. Battery state-of-health estimation: A step toward battery digital twins[J]. Electronics, 2024, 13(3): 587.

[5] Wongdet P, Boonraksa T, Boonraksa P, et al. Optimal capacity and cost analysis of battery energy storage systems in standalone microgrids considering battery lifetime[J]. Batteries, 2023, 9(2): 76.

[6] Stanchev P, Hinov N. Comparative Techno-Economic and Life Cycle Assessment of Stationary Energy Storage Systems: Lithium-Ion, Lead-Acid, and Hydrogen[J]. Batteries, 2025, 11(10): 382.

[7] Migliari L, Cocco D, Petrollese M. Levelized cost of storage (LCOS) of battery energy storage systems (BESS) deployed for photovoltaic curtailment mitigation[J]. Energies, 2025, 18(14): 3602.

[8] Mulder S, Klein S. Techno-economic comparison of electricity storage options in a fully renewable energy system[J]. Energies, 2024, 17(5): 1084.

[9] Issa R, Badr M M, Shalash O, et al. A data-driven digital twin for estimating the state-of-charge of electric vehicle lithium-ion batteries enabled by driving behavior application programming interfaces[J]. Batteries, 2023, 9(10): 521.

[10] Al-Shetwi A Q, Atawi I E, El-Hameed M A, et al. Digital Twin Technology for Renewable Energy, Smart Grids, Energy Storage, and Vehicle-to-Grid Integration: Advancements, Applications, Key Players, Challenges, and Future Perspectives in Modernizing Sustainable Grids[J]. IET Smart Grid, 2025, 8(1): e70026.

[11] Emrani A, Berrada A. A comprehensive review on the techno-economic assessment of hybrid energy storage systems integrated with renewable energy[J]. Journal of Energy Storage, 2024, 84: 111010.

[12] Iqbal H, Sarwar S, Kirli D, et al. A survey of second-life batteries based on a techno-economic perspective and application-based analysis[J]. Carbon Neutrality, 2023, 2(1): 8.

[13] Agajie T F, Ali A, Fopah-Lele A, et al. A comprehensive review on the techno-economic analysis and optimal sizing of hybrid renewable energy sources with energy storage systems[J]. Energies, 2023, 16(2): 642.

[14] Barata F, Sousa J, Viveiros C, et al. Techno-economic assessment of battery energy storage systems in renewable energy communities[J]. International Journal of Sustainable Energy Planning and Management, 2025, 44: 59–72.

[15] Agajie T F, Ibrahim F S, Amoussou I, et al. Comparative techno-economic analysis of grid-connected solar PV-battery and PV-fuel cell systems for sustainable academic laboratories in educational institutions[J]. Discover Sustainability, 2025, 6(1): 674.

[16] Chatzigeorgiou N G, Theocharides S, Makrides G, et al. A review on battery energy storage systems: Applications, developments, and research trends of hybrid installations in the end-user sector[J]. Journal of Energy Storage, 2024, 86: 111192.

[17] Adeyinka A M, Esan O C, Ijaola A O, et al. Advancements in hybrid energy storage systems for enhancing renewable energy-to-grid integration[J]. Sustainable Energy Research, 2024, 11(1): 26.

[18] Adeyemo A A, Tedeschi E. Technology suitability assessment of battery energy storage systems for high-energy applications on offshore oil and gas platforms[J]. Energies, 2023, 16(18): 6490.

[19] Tziovani L, Hadjidemetriou L, Timotheou S. Optimizing the bidding strategy and assessing the profitability of over-installed renewable plants equipped with battery energy storage systems[J]. Renewable Energy, 2024, 234: 121247.

[20] Khosravani A, Sieving J K, Billings B W, et al. Techno-economic analysis of long-duration energy storage integrated with high-penetration renewable energy systems[J]. Energy Reports, 2025, 14: 4086–4110.

[21] Barabino E, Fioriti D, Guerrazzi E, et al. Energy Communities: A review on trends, energy system modeling, business models, and optimization objectives[J]. Sustainable Energy, Grids and Networks, 2023, 36: 101187.

[22] Aranzabal I, Gomez-Cornejo J, López I, et al. Optimal management of an energy community with PV and battery energy storage systems[J]. Energies, 2023, 16(2): 789.

[23] Gwabavu M, Bansal R C, Naidoo R M. A review of onshore wind farm battery energy storage systems for techno-economic optimization[J]. International Journal of Modelling and Simulation, 2025, 45(6): 2237–2256.

[24] Borerwe C, Longe O M. Techno-economic analysis of large-scale battery energy storage systems for stationary applications in South Africa[J]. Engineering Research Express, 2025, 7(1): 012301.

[25] Adeyinka A M, Esan O C, Ijaola A O, et al. Advancements in hybrid energy storage systems for enhancing renewable energy-to-grid integration. Sustainable Energy Research, 11 (1)[EB/OL]. (2024)